Computer modelling and analysis of the photodegradation effect in a-Si:H p—i—n solar cell

2015 J. Semicond. 36 014002

(http://iopscience.iop.org/1674-4926/36/1/014002)

Computer modelling and analysis of the photodegradation effect in a-Si:H p–i–n solar cell

A.F Bouhdjar[1], L. Ayat[2], AM. Meftah[1, 3, †], N. Sengouga[1], and AF. Meftah[1]

[1]Faculté des Sciences, Laboratoire des Matériaux Semi-conducteurs et Métalliques, Université Mohammed Khider, B.P. 145, Biskra 07000, Algérie

[2]Laboratory of Semiconductor Devices Physics, Physics Department, University of Béchar, P.O. Box 417, Béchar 08000, Algeria

Abstract: Using a previous model, which was developed to describe the light-induced creation of the defect density in the a-Si:H gap states, we present in this work a numerical modelling of the photodegradation effect in the a-Si:H p–i–n solar cell under continuous illumination. We first considered the simple case of a monochromatic light beam with a wavelength λ between 530–540 nm non uniformly absorbed, then the global standard solar spectrum (AM 1.5) illumination is taken into account. The photodegradation is analysed on the basis of the resulting changes in the free carrier's densities, recombination rate, band structure, electrical potential and field, space charge, and current densities. Changes in the cell's external parameters: the open circuit voltage V_{oc}, the short circuit current density J_{sc}, the fill factor FF and the maximum power density P_{max} are also presented.

Key words: a-Si:H; Staebler–Wronski effect; p–i–n

DOI: 10.1088/1674-4926/36/1/014002 **EEACC:** 2520

1. Introduction

As is well known, the degradation of transport proprieties during illumination of the hydrogenated amorphous silicon (a-Si:H) materials, i.e., the so-called Staebler–Wronski effect (SWE)[1], is the main problem that limits the applicability of such materials in photovoltaic domains. The majority of models proposed to understand the microscopic mechanisms that cause this effect suggest that it is due mainly to a light-induced defect creation, stimulated by the non radiative recombination of the photogenerated free carriers. The energy released from such recombination can break weak bonds[2–6], or liberate bounded hydrogen atoms[6–10] that can diffuse and break weak bonds and then, further dangling bonds, i.e., defects, are created.

During illumination, the increase of the dangling bond density of states in the a-Si:H gap is obtained on the basis of our model of the light-induced defect creation in a-Si:H[11, 12]. The proposed model is based on experimental observation concerning the presence of the doubly hydrogenated weak SiSi bond (SiHHSi) configuration[6, 13], the hydrogen diffusion[14] and the main role of the hydrogen in the light-induced defect annealing[4, 5, 8–10]. The varying density of states is then used in the numerical modelling of the a-Si:H p–i–n solar cell, illuminated first with a monochromatic light beam (λ = 530–540 nm). The considered wavelength corresponds to the case of non uniform absorption (absorption coefficient $\alpha = 10^5$ cm^{-1}), which means an exponential decay of the generation rate away from the illuminated p-side of the device. Taking the photon flux ϕ equal to 10^{17} cm^{-2} s^{-1}, this gives an optical generation rate G in the photo-generation region equal to 10^{22} cm^{-3} s^{-1}, which is slightly lower than the value assured later by the total AM 1.5 spectrum illumination. We analyse the degradation in terms of the internal variables profile: the free carrier densities, recombination rates, space charges, band structure, potential, electrical field, and current densities. We also present the light-induced degradation effect on the cell photo-parameters, i.e. the open circuit voltage V_{oc}, the short circuit current density J_{sc}, the fill factor FF, and the maximum power density P_{max} .

2. SWE model

In our model[11, 12], the basic processes for light-induced creation of dangling bonds are given as follows: the defect creation occurs by a non radiative recombination between photoexcited electrons and holes at a weak SiSi bond adjacent to an SiHHSi bond. This can be justified by the fact that the majority of hydrogen is located in SiHHSi configurations rather than in isolated SiH bonds[6]. This weak SiSi bond is energetically favourable for recombination due to the additional stress imposed by the two hydrogen atoms. As a result of the released energy after recombination, one of the two hydrogen atoms moves to the site of the broken SiSi bond, forming two adjoining SiHD defects. The hydrogen atom is located at the tetrahedral site, rather than the bond centred site, of the broken SiSi bond, and the separation of the Si dangling bond and hydrogen atom is in the range 4–5 Å, which is consistent with ESR experiments[6]. The recombination at the SiHD defect site allows the production and diffusion of a mobile hydrogen atom through the material. If the dissociated hydrogen atom is inserted in the nearby SiHD defect, this will be annihilated and, in this case, there will be no defect creation and no SWE as a consequence. Thus, the hydrogen atom remains mobile until it meets a distant SiHD defect where they annihilate to form a SiHHSi bond. The hydrogen atom can also be re-trapped by col-

† Corresponding author. Email: amjad_meftah@hotmail.com
Received 15 July 2014, revised manuscript received 20 August 2014

liding with a second metastable H. In this case, both metastable Hs are trapped to form a SiHHSi bond again. The validation of our model[11, 12] has been fulfilled by the good agreement obtained between the defect creation kinetic simulation, based on rate equations describing the processes above, and the experimental data from Reference [9].

3. Physical model of the a-Si:H density of states

The typical density of localised states, $g(E)$, in the a-Si:H gap is comprised of the band tail state density, which decays exponentially from the band edge, and of the dangling bond state density. The latter is calculated according to the defect pool model improved by Powell and Deane[15].

The defect pool model has been proposed for the equilibrium properties of a-Si:H, which can account for a wide range of experimental results[15, 16]. The equilibration mechanism was identified as a conversion of weak bonds to dangling bonds according to the following reaction: SiHHSi + SiSi $\leftrightarrow$ 2SiHD[15]. The density of state distribution was determined by applying the law of mass action to both reactions: SiHD $\leftrightarrow$ SiSi + H and SiHHSi $\leftrightarrow$ SiSi + 2H, between the weak bond energy in the valence band tail and the energy level in the gap where the defect is formed. The density of state calculated within the framework of the defect pool model is expressed as follows[15]:

$$D(E) = \gamma \left[\frac{2}{f^{\mathrm{o}}(E)}\right]^{K_{\mathrm{B}}T^*/2E_{\mathrm{vo}}} P\left(E + \frac{\sigma^2}{2E_{\mathrm{vo}}}\right), \quad (1)$$

with

$$\gamma = \left(\frac{G_{\mathrm{v}} 2E_{\mathrm{vo}}^2}{2E_{\mathrm{vo}} - K_{\mathrm{B}}T^*}\right) \times \left(\frac{H}{N_{\mathrm{SiSi}}}\right)^{K_{\mathrm{B}}T^*/4E_{\mathrm{vo}}} \times \exp\left[\frac{-1}{2E_{\mathrm{vo}}}\left(E_{\mathrm{P}} - E_{\mathrm{v}} - \frac{\sigma^2}{4E_{\mathrm{vo}}}\right)\right],$$

where $P(E)$ is the defect pool function assumed to have a Gaussian distribution. σ and E_{p} are, respectively, the pool width and peak position. G_{v} and E_{vo} are, respectively, the density of states at E_{v} and the valence band tail width. T^* is the equilibrium temperature (freeze-in temperature) for which the density of states is maintained. H is the total hydrogen concentration and N_{SiSi} is the total electron concentration in the material. $f^{\mathrm{o}}(E)$ is the neutral dangling bond state occupancy.

Under illumination, the areas of defect Gaussian distributions increase similarly to the defect concentration N_{d} ($N_{\mathrm{d}} = \int_{E_{\mathrm{c}}}^{E_{\mathrm{v}}} D(E)\mathrm{d}E$), while their positions and widths remain unchanged. The valence and conduction band tails are supposed to be constants. These suppositions are made on the basis of experimental study performed by References [17, 18].

Figure 1 shows the evolution of the defect state density versus the illumination time, taking into account the assumptions above. The parameters used to calculate the defect density of states are listed in Table 1, and they give an initial (equilibrium, annealed) defect density N_{d} of 10^{16} cm^{-3}. Under illumination, the latter reaches 4×10^{16} cm^{-3} for a standard a-Si:H film soaked by a monochromatic light beam with an intensity of 10^{22} cm^{-3}s^{-1} and $\lambda < 570$ nm[9]. Afterwards, this density of states, varying with the illumination time, is implanted in the numerical modelling of the a-Si:H p–i–n solar cell to showing the related degradation effect on the internal variables as well as on the photo-parameters of the cell.

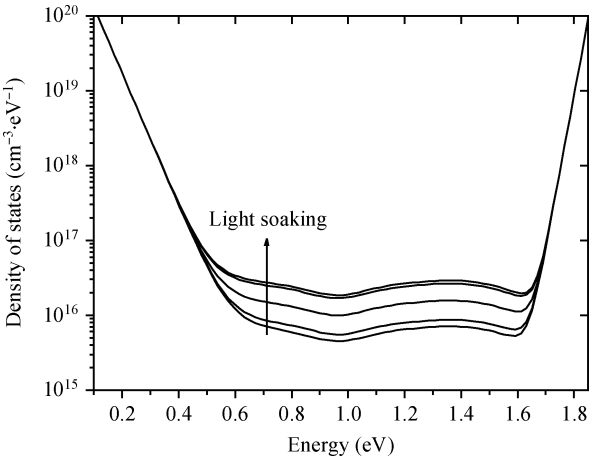

Figure 1. Light-induced increase of the density of state in the gap of the a-Si:H.

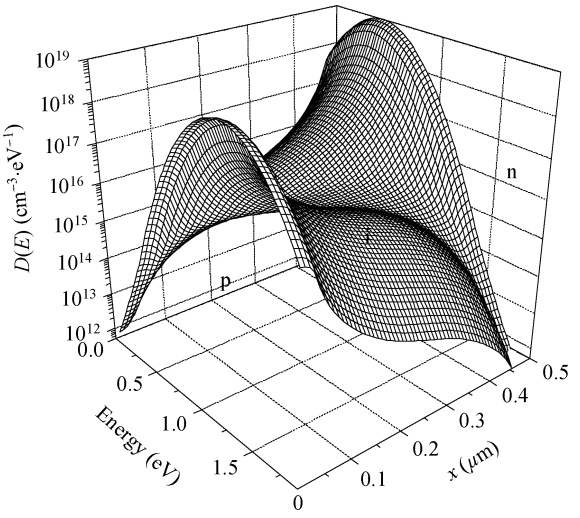

Figure 2. 3D variation of the defect state density.

4. Numerical model of the a-Si:H p–i–n cell

Our simulation program[19, 20] provides a one-dimensional numerical solution of the carrier transport problem in a-Si:H based p–i–n solar cell subject to equilibrium boundary conditions. Namely, a stationary simultaneous solution of Poisson's equation and the hole and electron continuity equations, approximated using finite difference[21, 22], is achieved taking into account the 3-D variation of $D(E)$ resulting from the spatial variation of the Fermi-level position within the energy gap (Figure 2)[19, 20]. The basic solution consists of the electric potential and the free carrier concentrations throughout the device. These results are complemented by the recombination rate, space charge density, electric field, hole and electron current density distributions within the device. The thicknesses of the p and n layers are both 0.01 μm and the whole device thickness is 0.5 μm. The transmittance T of the glass/TCO (transparent conductive oxide) substrate and the back reflection R of the n/metal contact are taken into account, the reason why the

Table 1. Simulation parameters of the physical and numerical models.

Parameter	Value
Pool width σ (eV)	0.19
Pool peak position E_p (eV)	1.27
Total hydrogen concentration H (cm^{-3})	5×10^{21}
Total electron concentration N_{sisi} (cm^{-3})	2×10^{23}
Defect state density freeze-in temperature T^* (K)	500
Characteristic temperature of the valence band tail T_v (K)	570
Characteristic temperature of the conduction band tail T_c (K)	246
Intrinsic Fermi level E_{fi} (eV)	0.98
p-layer thickness (nm)	10
i-layer thickness (nm)	480
n-layer thickness (nm)	10
Mobility gap, E_g (eV)	1.9
Activation energy in the p-layer, E_{fp} (eV)	0.28
Activation energy in the n-layer, E_{fn} (eV)	0.24
Density of states at E_c and E_v, G_c, G_v (cm^{-3} eV^{-1})	1×10^{21}
p- and n-layer doping densities, N_a, N_d (cm^{-3})	5×10^{18}
Annealed i-layer DOS (cm^{-3})	1×10^{16}
Free electron's mobility, μ_n (cm^2/(V·s))	20
Free hole's mobility, μ_p (cm^2/(V·s))	2
Capture coefficient of charged tail's states, C_{ct} (cm^3 s^{-1})	1×10^{-7}
Capture coefficient of neutral tail's states, C_{nt} (cm^3 s^{-1})	1×10^{-8}
Capture coefficient of charged dangling bond's states, C_{cd} (cm^3 s^{-1})	1×10^{-7}
Capture coefficient of neutral dangling bond's states, C_{nd} (cm^3 s^{-1})	1×10^{-8}
Glass/TCO substrate transmittance	0.9[25]
n/metal contact reflectivity	0.9[25]
Incident light beam wavelength λ (nm)	534
Incident light beam intensity ϕ (cm^{-2} s^{-1})	10^{17}
Absorption coefficient α (cm^{-1})	10^5

generation rate G distribution, in the monochromatic illumination case, is given by the following expression :

$$G(x) = T\alpha\phi \left\{\exp\left(-\alpha x\right) + R\exp\left[-\alpha\left(2d - x\right)\right]\right\}, \quad (2)$$

where α is the absorption coefficient, ϕ is the photon flux, and d is the thickness of the device.

The numerical solution is achieved using the simulation parameters listed in Table 1.

5. Results

Knowledge about the distribution of internal variables is important to understand the changes resulting from the light-induced degradation in the p–i–n device. To simulate the cell behaviour under the light-socked condition, the dangling bond density of states in the intrinsic layer (i-layer) has to be raised using our model of the light-induced defect increase in the gap states (Figure 1). As a result of the nonuniform light absorption, therefore non uniform generation, the light-induced increase in the dangling bond density (cm^{-3}) profile occurs inhomogeneously along the device (Figure 3).

Figure 4 shows the free electron and hole densities profiles obtained by simulation under the short circuit condition, at the annealed and degraded states. In the first case, the free hole density (p) dominates until 0.23 μm. Afterwards, the free electrons (n) become the dominating free charge carriers. In the degraded state, an important decrease in hole density occurs around the p–i interface. This is obvious since the defect density at the p–i interface is nearly four times greater than that

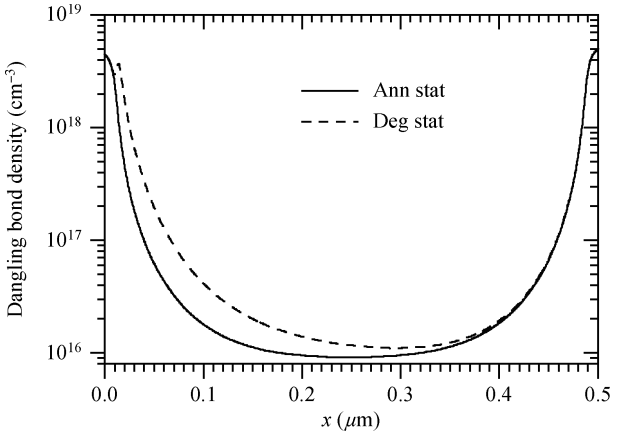

Figure 3. Dangling bond concentration profiles.

of the annealed state. Holes remain the dominating carriers but only until 0.07 μm, then electrons become the dominating free carriers for the remaining part of the device. Moreover, there is a considerable increase of electron and hole densities along the i-layer, which raises the $n \cdot p$ product. However, no further increase of the $n \cdot p$ product is expected at the i–n interface since there are no changes in n and p, while it decreases certainly at the p–i interface due to the important holes density decrease in this region.

Figure 5 shows the recombination rate profile at annealed and degraded states, and the generation rate profile. We remark that the recombination rate that was higher at the interface re-

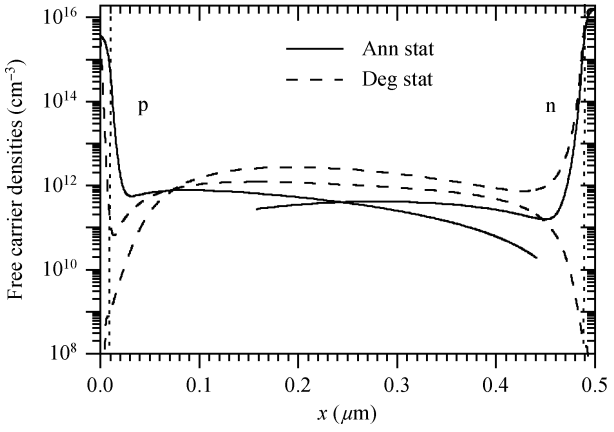

Figure 4. n and p density profiles, under short circuit condition.

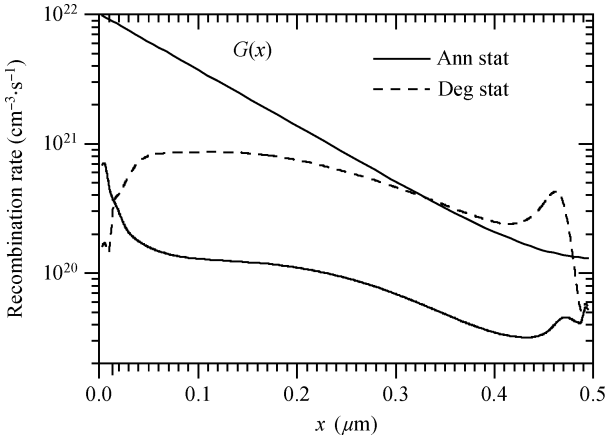

Figure 5. Generation and recombination rate profiles.

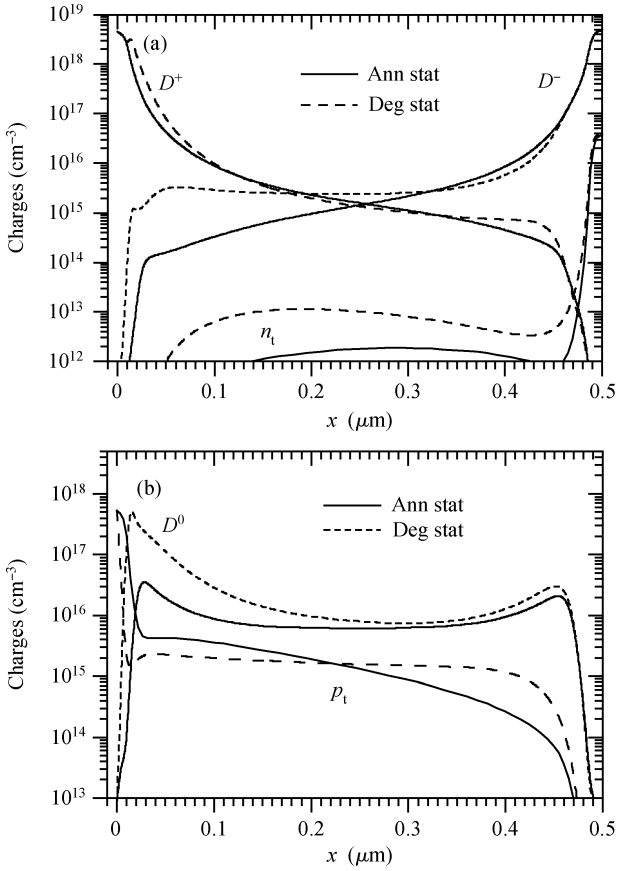

Figure 6. Trapped charge density profiles in band tails, p_t, n_t, and dangling bonds D^+, D^0, D^-.

gions in the annealed state decreases in the p-layer and at the p/i interface. This can be attributed to the important decrease of the free hole density in this region. In the rest of the device, there is however an increase in the bulk recombination related mainly to the increase of both n and p densities, except behind the i/n interface.

In Figures 6(a) and 6(b), the trapped charge is plotted at the different gap states in the annealed and degraded states. In the first case, the dominating charge in the front of the device is in D^+ (positively charged states of the dangling bond density of states). From 0.1 to 0.23 μm, the charge trapped in the valence band tail (p_t) contributes significantly to the positive charge, which dominates in this region. Beyond 0.3 μm, D^- (negatively charged states of the dangling bond density of states) take over as the dominating charged states, which leads to the sign reversal.

In the degraded state: D^- increases from the p–i interface up to 0.3 μm while it decreases slightly between 0.34 and 0.46 μm; p_t decreases from the p-edge to 0.2 μm and increases in the rest of the device; D^+ increases slightly except in the middle of the structure; D^o increases inhomogeneously, similarly to the dangling bond density profile; and finally n_t increases over nearly the totality of the device.

The augmentation of the negative charge in the region where the positive one dominates and vice versa, leads to the diminution of the space charge in the considered regions, and consequently, we expect that the electric field also decreases.

Figures 7–10 show respectively the band structure, the electric potential, the electric field and the space charge profiles, in both annealed and degraded states. From Figures 7(a) and 7(b), we see clearly that the light-induced defects cause an abrupt band bending near the p–i interface and consequently a very high electric field, while a low electric field in the i-layer is expected. Indeed, these two points are revealed in Figures 8 and 9. As shown in Figure 8, the potential profile in the degraded state varies strongly around the p–i interface while it becomes nearly constant along the i-layer. Examining Figure 9, showing the electric field profile, we see that the electric field increases from the edges of the device to the interfaces p–i and i–n, then it decreases towards the i-layer. The high interface fields are caused by the large space charge densities in the p and n layers (Figure 6). For the annealed state, if one referred to Figure 10, we find that the depletion regions resulting from the p–i and i–n interfaces meet at the i-layer. In the degraded state, a very high electric field indeed is found at the p–i interface, as expected above, while it decays through the i-layer and reaches 300 V/cm at 0.3 μm. This means that the depletion regions resulting from the p–i and i–n interfaces are well separated, and the field reverses immediately if a very small voltage bias is applied. The separation of the depletion regions is illustrated by Figure 10 and approves what has been advanced previously when we treated the trapped charge profiles in different gap states. The reduction of the electric field through the i-layer gives a reason for the increase of the free carriers in compari-

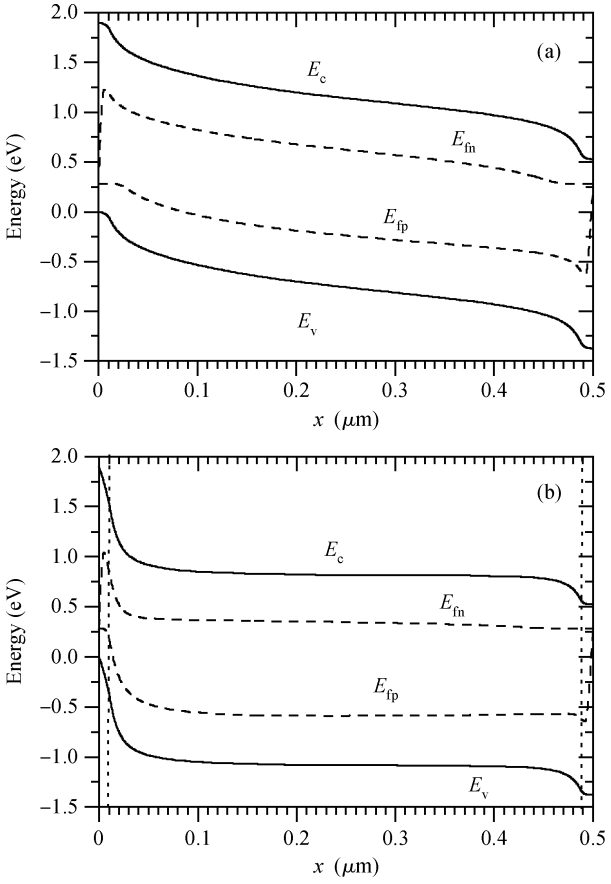

Figure 7. Gap structure, under short circuit condition in the (a) annealed state and (b) degraded state.

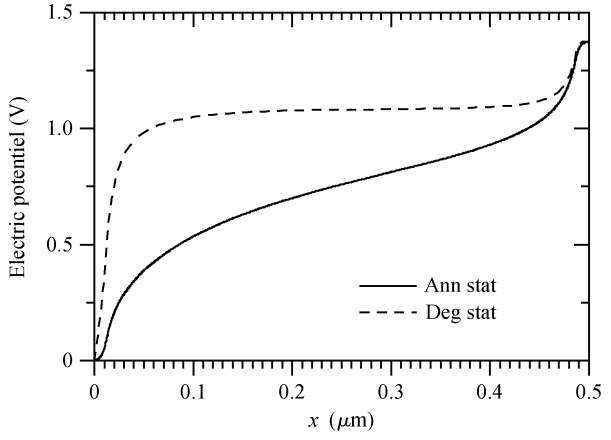

Figure 8. Electric potential profile, under short circuit condition.

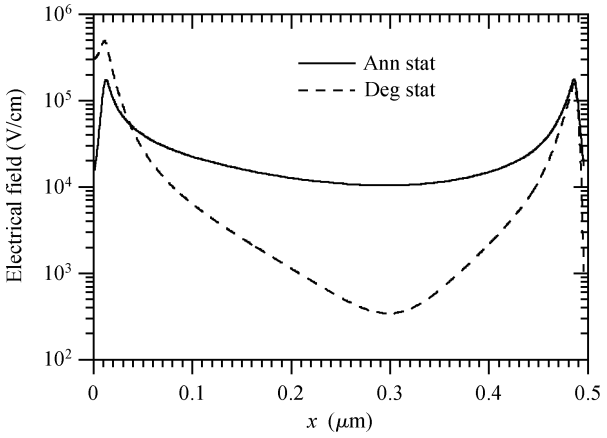

Figure 9. Electric field profile, under short circuit condition.

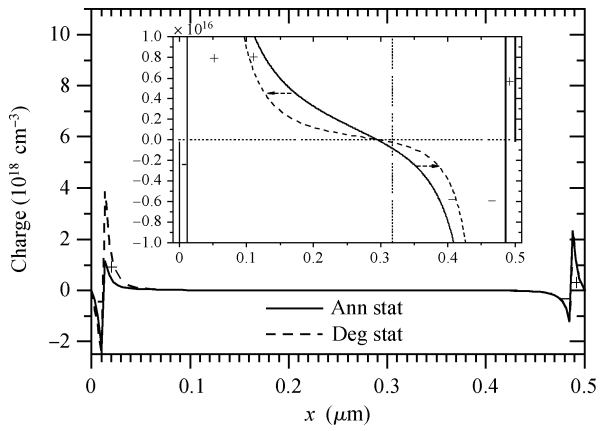

Figure 10. Space charge profile, under short circuit condition.

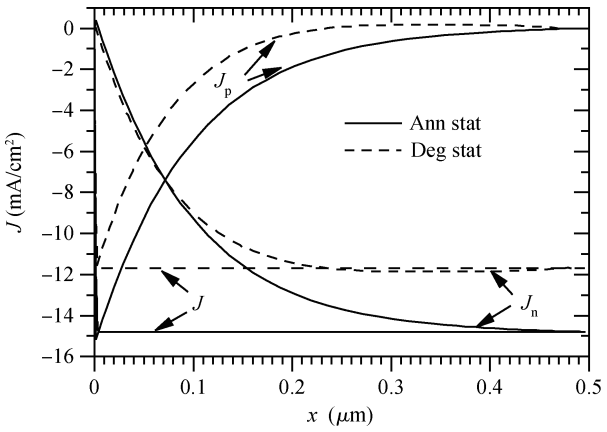

Figure 11. Electron and hole current densities' profiles.

son with the annealed state. Then, additional recombination is induced, which was indeed found from the recombination rate profiles (Figure 5).

Figure 11 shows electron, hole and total currents densities profiles calculated under short-circuit condition, at annealed and degraded states. A comparison of electron and hole currents densities, which are both negative, with the total current density shows that the current is mainly carried by electrons. Only in the region close to the p–i interface (0.07 μm in the annealed state, 0.05 μm in the degraded one), where the hole concentration is much higher than that of electrons, does the hole current density constitute the total current density. The degradation of the electron and the hole current densities is clearly shown and causes the decrease of the total current density from 14.79 to 11.68 mA/cm^2. Moreover, we remark that there is a very weak decrease in both electron and hole current density profiles from 0.44 μm at the degraded state. This is explained by the recombination rate, which locally exceeds the generation rate, as can be seen if one refers again to Figure 5. In order to analyze in more detail the transport mechanism, in Figures

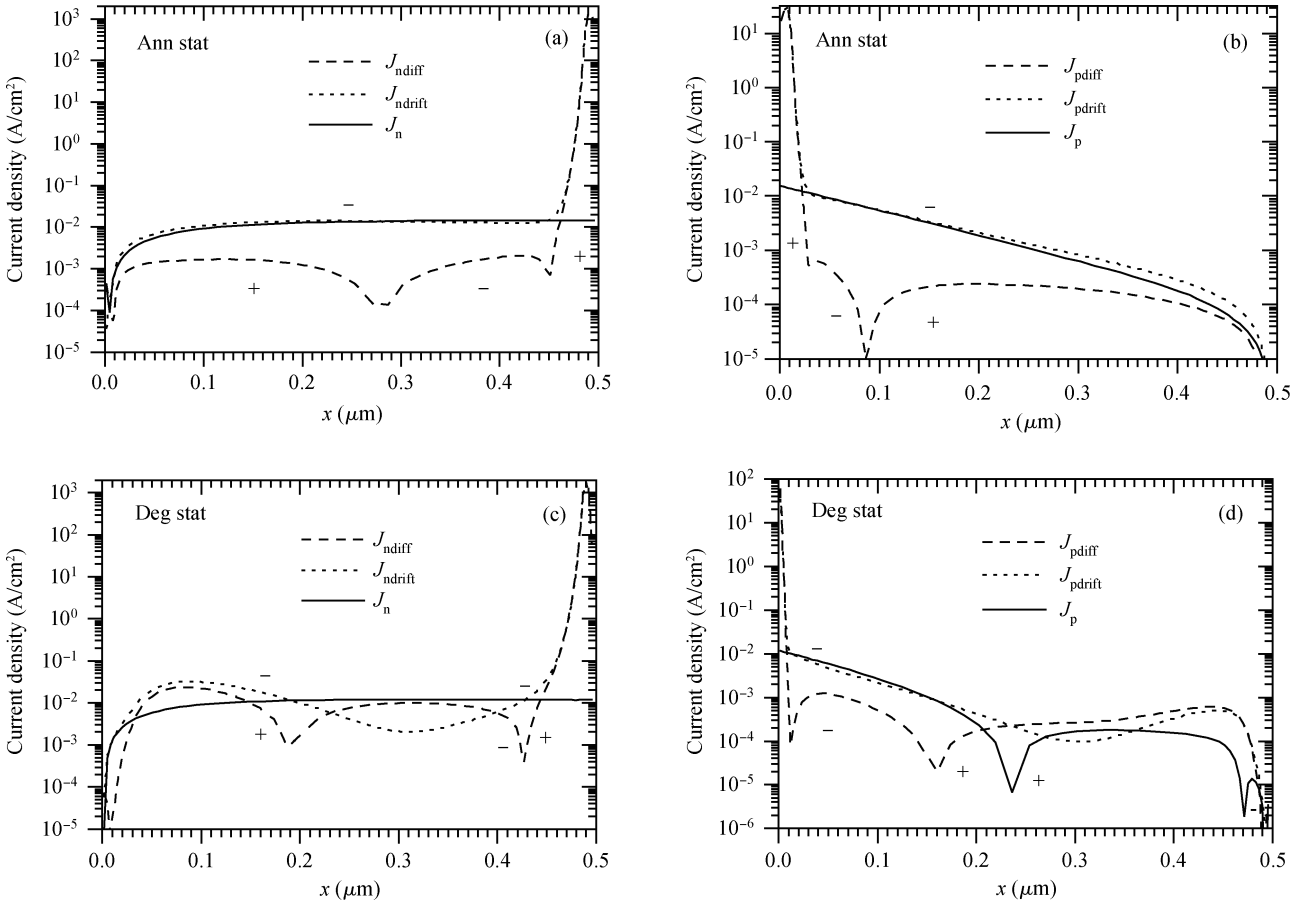

Figure 12. (a) Drift- and Diffusion-electron current density profiles in annealed state, (b) drift- and diffusion-hole current density profiles in the annealed state, (c) drift- and diffusion-electron current density profiles in the degraded state, and (d) drift- and diffusion-hole current density profiles in the degraded state.

Table 2. The cell photo-parameter degradation when $\mu_n/\mu_p = 20/2$ (cm^2/(V·s)) and $\mu_n/\mu_p = 25/6$ (cm^2/(V·s)).

μ_n/μ_p 20/2	J_{sc} (mA/cm^2)	V_{oc} (V)	FF	P_{max} (mW/cm^2)	μ_n/μ_p 25/6	J_{sc} (mA/cm^2)	V_{oc} (V)	FF	P_{max} (mW/cm^2)
Ann state	14.79	0.975	0.58	8.46	Ann state	15.08	0.972	0.652	9.65
Deg state	11.68	0.9	0.50	5.27	Deg state	14.5	0.915	0.56	7.43
	ΔJ_{sc} %	ΔV_{oc} %	Δ FF %	ΔP_{max} %		ΔJ_{sc} %	ΔV_{oc} %	Δ FF %	ΔP_{max} %
	−21	−7.69	−14.86	−37.81		−4.11	−5.86	−14.27	−22.61

12(a)–12(d), electrons and holes current densities are separated into drift and diffusion components. For both annealed and degraded states, the majority carriers current densities compete between drift and diffusion in the very front of the sample (close to the p–i interface) as in the back (close to the i–n interface). In the very front of the sample, the hole current, mainly drift current (since the hole current density is negative like the drift one), dominates. Similar results hold for electrons in the back of the device. We note here that an exception in the degraded state is found for holes at the p–i interface, where there is a large decrease of the free holes density, which are captured by the high D^+ density, compared to the annealed state (Figure 4). Consequently, the hole-diffusion current density decreases significantly and the transport process remains drift-dominated in this region.

Throughout the i-layer, for electrons as for holes, the drift current density (negative) is the dominant partial current density in the annealed state, for which the electric field strength is high in the active region. However, the competition between the drift and diffusion current densities persists in the degraded state. The region where the diffusion current density dominates the electric field is low, thus weakening the drift current density.

We summarized in Table 2 the photodegradation effect on the output parameters of the cell, and also the effect of increasing the free carrier mobilities μ_n and μ_p, given in more detail in a previous work[23].

For a good solar cell, a fill factor of more than 0.65 can be expected. In the $\mu_n/\mu_p = 20/2$ case of Table 2, the FF is relatively low because the dangling bond density of states is calculated before the degradation, according to the defect pool model improved by Powell and Deane[15]. The presence of the doubly hydrogenated weak SiSi bond (SiHHSi) configuration[6, 13], the hydrogen diffusion, and the carrier life time be-

Table 3. The solar cell output parameters under the full solar spectrum (AM 1.5) illumination in the annealed and degraded states.

μ_n/μ_p 20/2	J_{sc} (mA/cm^2)	V_{oc} (V)	FF	P_{max} (mW/cm^2)
Ann state	16.73	0.975	0.58	9.46
Deg state	12.63	0.9	0.50	5.68

ing much shorter than the transit time (when there is no applied reverse bias as in a-Si:H solar cell case), all this contributes to making recombination the governing behaviour of the device, and a relatively low fill factor can be expected. However, the 0.58 value for the FF is better than the other simulation works that used the defect pool model; as an example, we can refer to values of $\sim$ 0.4 to 0.425 obtained in Gao works[24]. We also indicate that the 0.58 value for the FF remains in the experimental range, as noted in many works[25–27] realised with conditions close to those of the current manuscript. Although the fill factor is relatively low, the short-circuit current density has an improved value in the annealed state.

Finally, we present in Table 3 the solar cell output parameters at the annealed state and degraded state, obtained under the global standard solar spectrum (AM 1.5) illumination and using the measured data corresponding to the full spectrum AM 1.5 for the absorption coefficient, given in Reference [28]. Relative to the monochromatic light case, a pretty increase is noted in the short-circuit current density and also in the maximum power density provided by the cell for both cases: annealed state and degraded state.

6. Conclusion

Our model of the light-induced defect creation together with the numerical modelling of the a-Si:H p–i–n solar cell have been used to provide a better understanding of the physical mechanisms governing the operation and the degradation of the device under illumination. In this approach, we first considered the simple case of a monochromatic light beam nonuniformly absorbed; this leading to an exponentially decreasing generation rate from the illuminated p-side to the n-side of the device. We have interpreted our results on the basis of an inhomogeneous increase of the dangling bond defect distribution, as a consequence of the degradation effect related to the absorbed light profile in the i-layer. Such a distribution induces important changes in the internal variable profiles and the external photo-parameters of the device. These changes can be summarised as follows.

(1) An important increase in recombination rate, due mainly to the increase of the bulk $n \cdot p$ product, is the reason why the current density decreases considerably along the device.

(2) An abrupt band bending through the p-side causes a high electric field in this region, while a low electric field is found in the i-layer. The latter further encourages the bulk recombination of free carriers.

(3) The carrier diffusion current densities across the i-layer, neglected in the annealed state, contribute significantly to the total current density (mainly the electron diffusion current).

(4) Decreases occur in the photo-parameters, which can be visualised in terms of percentages: 21% in J_{sc}, 7.69% in V_{oc}, 14.86% in FF and 37.81% in P_{max}. The increase of μ_n from 20 to 25 cm^2/(V·s) and μ_p from 2 to 6 cm^2/(V·s) improves the cell photo-parameters and minimizes significantly their deteriorations: 4.11% in J_{sc}, 5.86% in V_{oc}, 14.27% in FF and 22.61% in P_{max}.

Finally, the results are expanded to the full spectrum AM 1.5 condition of illumination under which the a-Si:H solar cell usually operates. Relative to the monochromatic light case, an increase is noted in the short-circuit current density and also in the maximum power density provided by the cell for both cases: annealed state and degraded state.

References

[1] Staebler D L, Wronski C R. Reversible conductivity changes in discharge-produced amorphous Si. Appl Phys Lett, 1977, 31: 292
[2] Stutzmann M, Jackson W B, Tsai C C. Light-induced metastable defects in hydrogenated amorphous silicon: a systematic study. Phys Rev B, 1985, 32: 23
[3] Wu Z Y, Siefert J M, Equer B. Preparation and physical properties of RF-sputtered amorphous films in the Al_2O_3/AlN system. J Non-Cryst Solids, 1991, 137/138: 227
[4] Biswas R, Pan B C. Defect kinetics in new model of metastability in a-Si:H. J Non-Cryst Solids, 2002, 299–302: 507
[5] Morigaki K, Hikita H. Model of the light-induced creation of two types of dangling bonds in a-Si:H. J Non-Cryst Solids, 2000, 266–269: 410
[6] Powell M J, Wehrspohn R B, Deane S C. Nature of metastable and stable dangling bond defects in hydrogenated amorphous silicon. J Non-Cryst Solids, 2002, 299–302: 556
[7] Jackson W B. Role of hydrogen complexes in the metastability of hydrogenated amorphous silicon. Phys Rev B, 1990, 41: 10257
[8] Godet C, Cabarrocas P R I. Role of Si–H bonding in a-Si:H metastability. J Appl Phys, 1996, 80: 97
[9] Godet C. Metastable hydrogen atom trapping in hydrogenated amorphous silicon films: a microscopic model for metastable defect creation. Philos Mag B, 1998, 77: 765
[10] Branz H M. The hydrogen collision model: theory and experiment. J Non-Cryst Solids, 2000, 266–269: 391
[11] Meftah A F, Meftah A M, Merazga A. A theoretical study of light induced defect creation, annealing and photoconductivity degradation in a-Si:H. J Phys: Condens Matter, 2004, 16: 3107
[12] Meftah A F, Meftah A M, Merazga A. Modelling of Staebler-Wronski effect in hydrogenated amorphous silicon under moderate and intense illumination. Defect and Diffusion Forum, 2004, 230–232: 221
[13] Han D. Search for the factors determining the photodegradation in high efficiency a-Si:H solar cells. Report NREL/SR-520-31754, 2002
[14] Cheong H M, Lee S H, Nelson B P, et al. Light-induced long-range hydrogen motion in hydrogenated amorphous silicon at room temperature. Appl Phys Lett, 2000, 77: 2686
[15] Powell M J, Deane S C. Defect-pool model and the hydrogen density of states in hydrogenated amorphous silicon. Phys Rev B, 1996, 53: 10121
[16] Powell M J, Deane S C. Improved defect-pool model for charged defects in amorphous silicon. Phys Rev B, 1993, 48: 10815
[17] Schmidt J A, Arce R, Buitrago R H, et al. Light-induced defects in hydrogenated amorphous silicon studied by the constant-photocurrent method. Phys Rev B, 1997, 55: 9621
[18] Schmidt J A, Arce R D, Koropecki R R, et al. Light-induced creation of metastable defects in hydrogenated amorphous silicon

studied by computer simulations of constant photocurrent measurements. Phys Rev B, 1999, 59: 4568

[19] Meftah A M, Meftah A F, Hiouani F, et al. Numerical simulation of the defect density influence on the steady state response of a silicon-based p–i–n cell. J Phys: Condens Matter, 2004, 16: 2003

[20] Meftah A M, Meftah A F, Merazga A. Numerical simulation and analysis of the dark and illuminated $J–V$ characteristics of a-Si-H p–i–n diodes. J Phys: Condens Matter, 2006, 18: 5459

[21] Kurata M. Numerical analysis for semiconductor devices. MA Heath, Lexington, 1982

[22] Selberherr S. Analysis and simulation of semiconductor devices. Springer, Berlin, 1984

[23] Meftah A F, Meftah A M, Belghachi A. Computer simulation of the a-Si:H p–i–n solar cell performance sensitivity to the free carrier's mobilities, the capture cross sections and the density of gap states. J Phys: Condens Matter, 2006, 18: 9435

[24] Gao W. Computer modelling and experimental characterisation of amorphous semiconductor thin films and devices. PhD Thesis, University of Abertay, Dundee, 1995

[25] Khan P A R, Butta S M, Malik S A. Modeling of transport properties of amorphous silicon solar cells. IJAP, 2010, 6(1): 25

[26] Dutta U, Chatterjee P, Tchakarov S, et al. Metastable defect migration under high carrier injection in hydrogenated amorphous silicon p–i–n solar cells. J Appl Phys, 2005, 98: 044511

[27] Raniero L, Martins N, Canhola P, et al. Influence of the layer thickness and hydrogen dilution on electrical properties of large area amorphous silicon p–i–n solar cell. Solar Energy Materials & Solar Cells, 2005, 87: 349

[28] Dawson R M, Li Y, Gunes M, et al. Optical properties of component materials in multi-junction hydrogenated amorphous silicon based solar cells. Proc 11th EC Photovoltaic Solar Energy Conference, Montreux, Switzerland, 1992: 680